

Supporting Information

Spacer defined intrinsic multiple patterning

Sophia K. Laney,^{1‡} Tao Li,^{1‡} Martyna Michalska,^{1‡} Francisco Ramirez,¹ Mark Portnoi,¹ Junho Oh,² Manish K. Tiwari,^{2,3} Iain G. Thayne,⁴ Ivan P. Parkin,⁵ and Ioannis Papakonstantinou^{1}*

¹Photonic Innovations Lab, Department of Electronic & Electrical Engineering, University College London, Torrington Place, London WC1E 7JE, UK

²Nanoengineered Systems Laboratory, Department of Mechanical Engineering, University College London, Torrington Place, London WC1E 7JE, UK

³Wellcome/EPSRC Centre for Interventional and Surgical Sciences (WEISS), University College London, London, W1W 7TS, UK

⁴James Watt School of Engineering, University of Glasgow, Glasgow G12 8LT

⁵Department of Chemistry, University College London, Torrington Place, London WC1E 7JE, UK

‡ These authors contributed equally

* Authors to whom correspondence should be addressed

Email: i.papakonstantinou@ucl.ac.uk

Table of content:

Supporting Methods	Page
Laser Interference Lithography	4
Fabrication process for one SDIMP iteration in SiO ₂	4
Replication into polymers	5
Supporting Text	
Text S1 – Future outlook: fabrication	5
Text S2 – Future outlook: applications	6

Supporting Figures	Page
Figure S1 – <i>Schematics highlighting the differences between SDIMP and SDDP/D-SDDP methods</i>	7
Figure S2 – <i>Library of feasible structure arrays by SDIMP method</i>	8
Figure S3 – <i>Corresponding SEM images to the fabrication scheme (steps 1-6) in Figure 1a</i>	9
Figure S4 – <i>Corresponding SEM images to the fabrication scheme (steps 1-6) in Figure 1b</i>	10
Figure S5 – <i>SEM images of the temporal evolution of nanotubes during step 5 to 6 of the fabrication process</i>	11
Figure S6 – <i>Laser interference lithography</i>	12
Figure S7 – <i>Corresponding SEM images (45° tilted) to the fabrication of nanotubes in glass</i>	13
Figure S8 – <i>Representative nanotube structures imprinted in polymers</i>	14
Figure S9 – <i>SEM images of nanotubes generated at two different pitches</i>	15
Figure S10 – <i>Investigation into the effect of coil power, platen power and time for the fabrication of the nanohole arrays in Si</i>	16
Figure S11 – <i>Tuning the transfer of the crown structure to the nanotube, and the outer and inner tapering</i>	17
Figure S12 – <i>Further nanostructures generated through two SDIMP iterations</i>	18
Figure S13 – <i>Schematics for the fabrication of hierarchical structures through two SDIMP iterations</i>	19

Figure S14 – <i>Optical properties of the tapered nanotube with a top crown at oblique angle of incidence</i>	20
Supporting Tables	
Table S1 – <i>Nanotube dimensions</i>	21
Table S2 – <i>Nanotube fabrication: (i) etching times and (ii) thicknesses of SiO₂ or Al₂O₃ deposition</i>	21
Table S3 – <i>Nanotube etching conditions – Oxford RIE</i>	22
Table S4 – <i>Nanotube etching conditions – ICP STS</i>	22
Table S5 – <i>Tunability at each step of the SDIMP process</i>	23
Table S6 – <i>Etching rates of single nanotubes starting from nanoholes and nanopillars corresponding to Figure 1</i>	24
Table S7 – <i>Iterative SDDP structure fabrication</i>	25
<i>References</i>	26

Supporting Methods

Laser interference lithography

The substrates are patterned using laser interference lithography (LIL) to achieve on-demand, periodically ordered photoresist nanopillars or nanoholes of precise pitch and excellent uniformity. Whilst many established lithography methods are available, LIL has many advantages as it is a facile maskless technique as well as inexpensive and scalable.¹

LIL relies on the interference between two or more coherent beams of radiation to create spatially periodic regions of high and low intensity light. These regions are recorded within a photosensitive layer before being developed. We convincingly demonstrate excellent pattern integrity over several centimetres on fused silica (Figure S6a). Using a one-mirror Lloyd's interferometer set up, the pitch of the nanopattern is dictated by the wavelength of the laser, the angle of intersection between mirror, sample and stage orientation, with respect to direction of laser beam according to Equation S1:²

$$P = \frac{\lambda}{2 \sin \theta} \quad [\text{Eq. S1}]$$

Square packed nano-pillars and -holes were generated by exposing a negative photoresist twice with a 90°-rotation of the sample after the first exposure. Hexagonally close packed (hcp) arrays were also obtained either by a 60°-rotation or using a two-mirror interferometer set up. The simulated intensity profiles for the one- and two-mirror system can be seen in Figure S6b,c.

Fabrication process for one SDIMP iteration in SiO₂

The fabrication process can be extended to glass nanotube arrays, and is shown schematically with corresponding SEMs in Figure S7. The same steps are taken as with Si, however no hard mask is required as the etching contrast between photoresist and glass is much higher than that of photoresist and silicon. As before, nanohole arrays were fabricated in photoresist *via* LIL. To register the pattern into the underlying SiO₂, a brief oxygen plasma was applied to remove residual photoresist, followed by plasma etching in CHF₃/Ar. The attained glass nanohole arrays were coated in a conformal layer (30 nm) of Al₂O₃ *via* ALD. To reveal the Al₂O₃ tube, a Cl plasma breakthrough etch was applied. Unlike fluorine-based plasma which results in non-volatile AlF₃ generation that can re-deposit during the process, use of chlorine overcomes the

issue by leading to formation of volatile products; AlCl_3 or Al_2Cl_6 . Subsequent SiO_2 etching was performed under CHF_3/Ar plasma using the Al_2O_3 spacer as a mask.

Replication into polymers

Having fabricated the structures in a hard material, the pattern can be readily replicated into polymers. This can be performed *via* soft lithography to generate flexible nanostructured substrates with the precise dimensions and morphology controlled through the SDIMP process. Soft lithography also allows for the inverse morphology to be obtained which can give rise to otherwise hard to achieve structures (hierarchical). The case is demonstrated in Figure S8a, where inverse nanotubes were generated in polyurethane acrylate (PUA) from nanotubes with $h_i > h_o$. Alternatively, demonstrated in Figure S8b is the replication of the nanotube array into PR *via* nanoimprint lithography (NIL). The PR nanotubes can subsequently be etched directly into the underlying substrate, mitigating the need for the ALD/etching process once a master with the desired features has been fabricated. NIL also allows for much larger scale and facile fabrication with the potential for roll-to-roll processing.

Supporting text

Text S1. Future outlook: fabrication

The versatility of SDIMP stems from the vast availability of photolithographic and self-assembly (*e.g.*: UV-lithography, direct laser writing, 2-photon polymerisation, block copolymer and nanosphere lithography *etc.*) methods for initial patterning, in addition to numerous target material-spacer pairs of high etching contrast (selectivity $>10:1$) at various RIE processes. For example, Williams *at al.* provides 620 etch rates of 53 materials in popular etching processes which serves well as a guide for the process design³. This allows for nearly no limit on feature dimensions and spatial arrangement, nor on material choice. For example, one of the attractive future directions would be exploiting block copolymer (BCP) self-assembly to migrate the process to the sub-100 nm and even the sub-10 nm regimes. Besides, the multiple self-assembly is gaining a lot of attention,⁴ and it could further diversify the 2D and 3D geometries of the patterns. While our proof-of-concept work features periodic arrays, there are no barriers to fabricating semi-random or even completely random structures. The degree of order is engraved in the first step of the process (photoresist patterning) and well-known methods such as electron beam lithography or focused ion beam, among others, could be used to create free-form patterns.

Alternatively, a change of the initial order can be further explored by means of the SDIMP process similarly to an example given in Figure S2. There, a formation of connected and binary nanoarrays elicits changes in the spatial arrangement such that square-packed nanostructures become (compressed) hexagonally-packed.

Moreover, the method could readily be expanded to other semiconducting (*e.g.*: Ge, GaAs, InP, ZnO *etc.*), oxide (*e.g.*: HfO₂, ZrO₂, TiO₂, MgO, and Sc₂O₃ *etc.*) and nitride materials (SiN). Note, for low selectivity pairs, *e.g.*, TiO₂-silicon processed under chlorine plasma⁵, for instance, the SDIMP is possible but will result in low aspect ratio structures.

If, however, a free-standing TiO₂ nanostructure is needed, one could use our reported process to generate a sacrificial template of a given complexity in silicon. Subsequently, one could deposit TiO₂ onto the template and perform SF₆ isotropic etching (selectivity as high as 66,000:1) to completely remove the sacrificial layer, resulting in the TiO₂ complex pattern⁶.

Text S2. Future outlook: applications

In addition to the demonstrated applications, we believe our work will benefit many other fields of use. For example, we report structures formed through a double SDIMP iteration in Figure S12, where sub-10 nm gaps between rings were successfully attained. These very small gaps are highly desired for application in optical trapping, whereby micro-/nanoscopic objects are physically held and moved with nanometric position using a highly focussed laser beam.^{7,8} Moreover, for aperture based nano-optical tweezers, ultranarrow slits on the order of tens of nanometers are beneficial for boosting the efficiency, signifying the potential of this technique for optical trapping.⁹⁻¹¹ Another prospective application of the achievable structures through SDIMP, is Surface-Enhanced Raman Scattering (SERS). Through metallisation of our structures, surface plasmons can be channelled or concentrated to greatly enhance the signal when detecting single molecules. Alternatively, they can be used to generate smooth patterned metals *via* known template stripping technique, which utilizes the phenomenon of the poor adhesion and good wettability of noble metals on glass or silicon.¹²

Owing to the myriad of structural combinations, spatial arrangements and material choice mentioned previously, SDIMP speaks to many more fields and we foresee its application spanning metamaterials, biotechnology, sensing, batteries, DRAM memories, drug delivery systems, nanocatalysis, and plastic electronics (*via* replication in polymers) amongst others.

Supporting figures

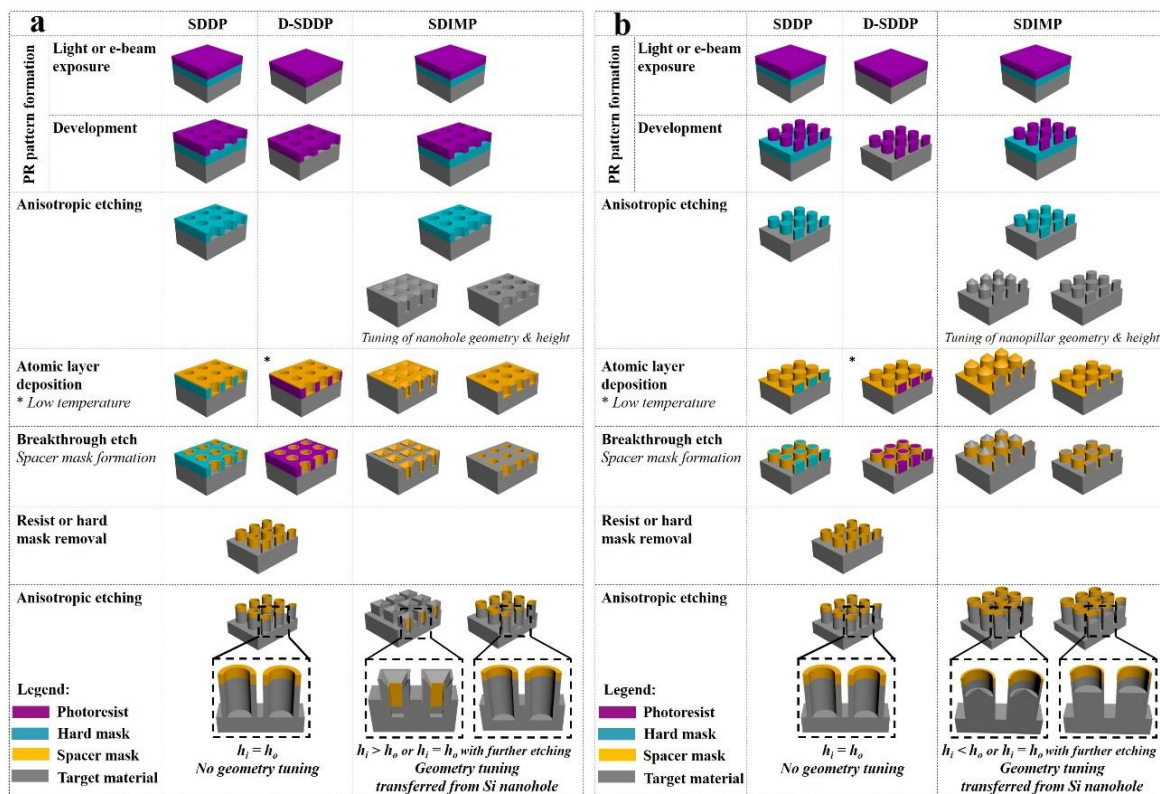

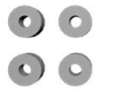


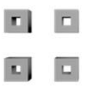


















Figure S1. Schematics highlighting the differences between SDIMP and SDDP/D-SDDP methods for circular patterns. Here, SDIMP is spacer defined intrinsic multiple patterning; SDDP is spacer defined double patterning; and D stands for direct. **(a)** Starting from a nanohole morphology and **(b)** starting from a nanopillar morphology in PR. In SDIMP, the pattern is transferred from the hard mask to the target material *via* anisotropic etching, whereby tuning of the morphology can be introduced [(a) square with crown, or circular nanoholes and (b) nanopencils or flat nanopillars]. The ALD-deposited spacer is then applied directly onto the pre-patterned target material, resulting in the conformal layer following the tuned nanohole/pillar geometry. As shown, this is not possible for either SDDP or D-SDDP as the nanohole/pillar pattern is only transferred to the hard mask or PR, respectively. The subsequent etching of the ALD-coated nanostructures results in nanotubes with, for SDIMP varying inner and outer height with possible extension to equal heights, whereas for SDDP and D-SDDP typically nanotubes with equal heights are achieved (modifications in some cases are possible, however the control is poor).

a	Cylindrical square packed tubes			Cuboid square packed tubes			Cylindrical hexagonally packed tubes
One iteration							
Two iterations	Thin 	Thin 	Thin 	Thin 	Thin 	Thin 	Thin 
Thick							

b

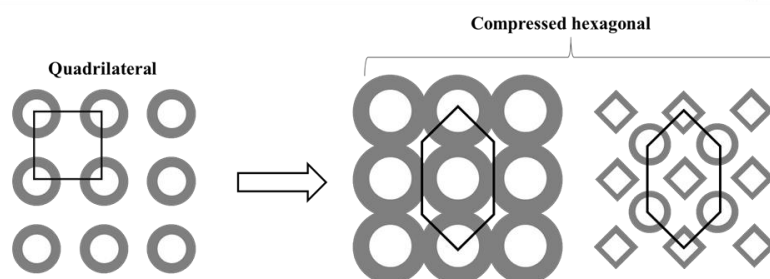


Figure S2. Library of feasible structure arrays by SDIMP method. (a) One iteration results in cylindrical or cuboid square packed tubes, or cylindrical hexagonally packed tubes. Through the second iteration of the SDIMP process, various complex nanostructures can be attained. (b) An alteration in the spatial arrangement from square to (compressed) hexagonally packed, through the generation of connected and binary nanoarrays.

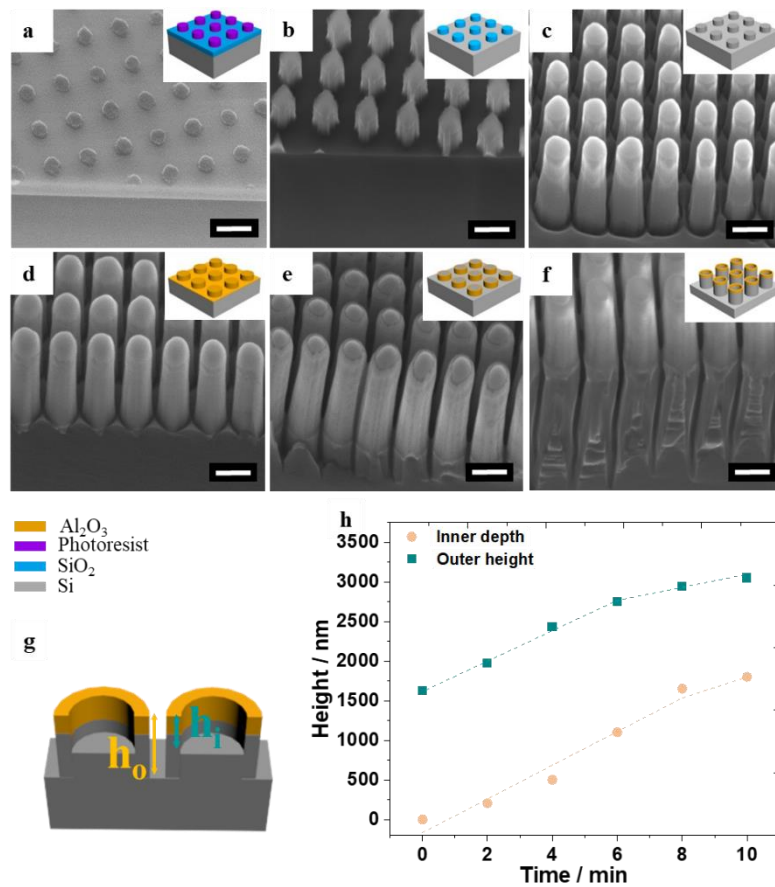


Figure S3. Corresponding SEM images (45° tilted) to the fabrication scheme in Figure 1a when starting from photoresist nanopillar morphology. (a) Photoresist pattern. (b) Etching the underlying SiO₂ layer using the photoresist mask. (c) Etching silicon using the SiO₂ as a hard mask. (d) Depositing conformal layer of aluminium oxide *via* ALD. (e) Etching Al₂O₃ to the point where the horizontal deposition is consumed and only vertical deposition remains. (f) Etching into silicon using the vertical deposition as a mask. (g) Schematic indicating how the evolution of the inner and outer height was measured in (h) in which we present how these heights change for a nanotube originating from a pillar, which possesses an inherently larger initial h_o than h_i . Scale bar = 500 nm.

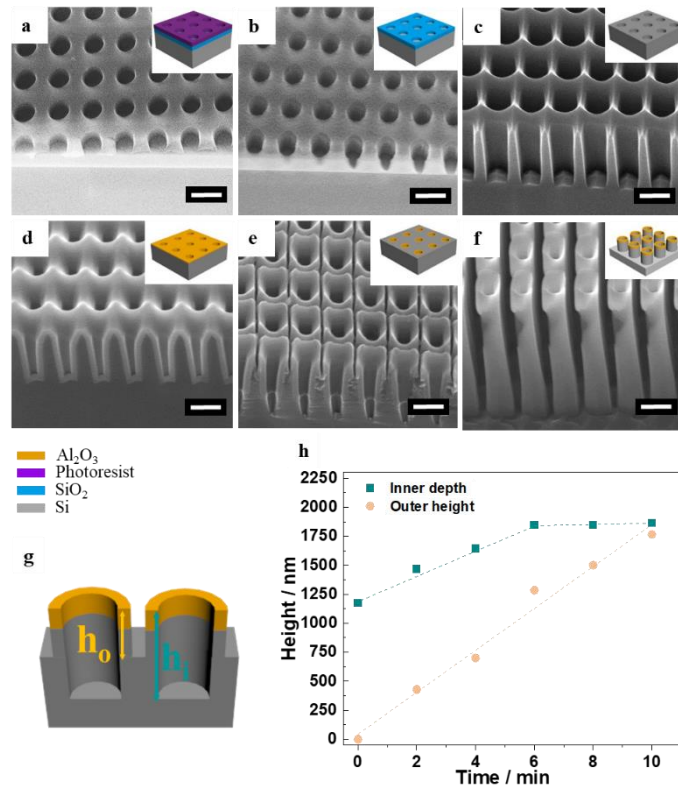


Figure S4. Corresponding SEM images (45° tilted) to the fabrication scheme in Figure 1b when starting from photoresist nanohole morphology. (a) Photoresist pattern. (b) Etching the underlying SiO₂ layer using the photoresist mask. (c) Etching silicon using the SiO₂ as a hard mask. (d) Depositing conformal layer of aluminium oxide *via* ALD. (e) Etching Al₂O₃ to the point where the horizontal deposition is consumed and only vertical deposition remains. (f) Etching into silicon using the vertical deposition as a mask. (g) Schematic indicating how the evolution of the inner and outer height was measured in (h) in which we present how these heights change for a nanotube originating from a hole, which possesses an inherently larger initial h_i than h_o. Scale bar = 500 nm.

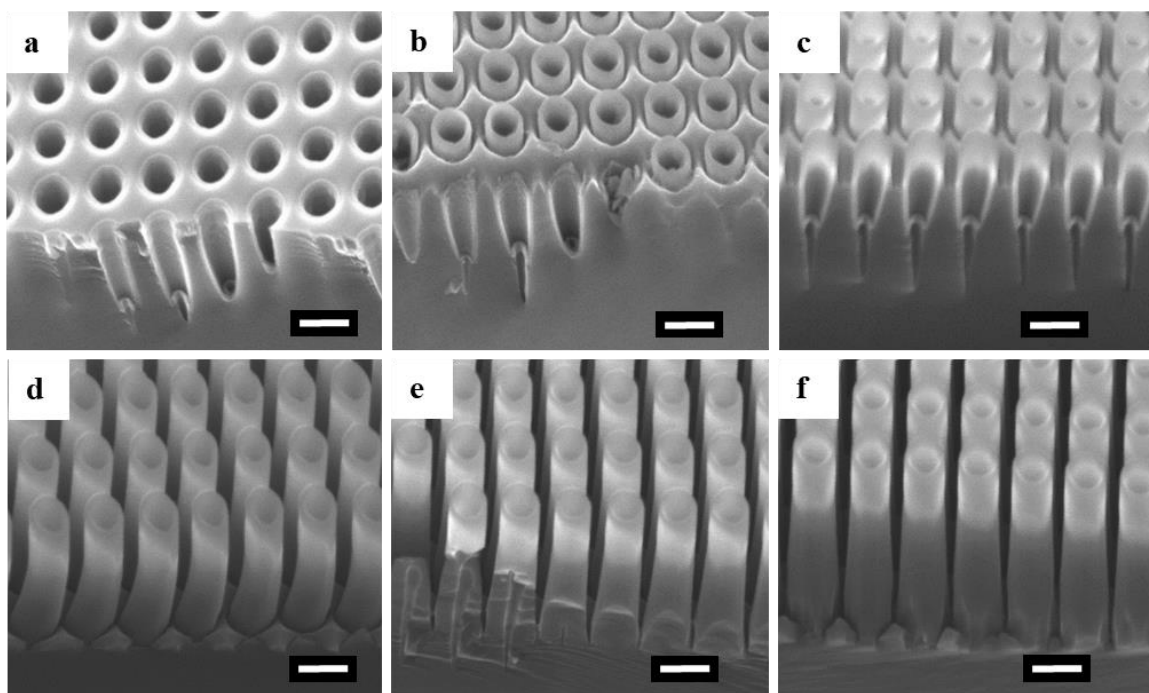


Figure S5. SEM images of the temporal evolution of nanotubes during step 5 to 6 of the fabrication process. Increasing etch time in minutes: (a) 6 min; (b) 8 min; (c) 10 min; (d) 12 min; (e) 14 min; (f) 16 min. Scale bar = 500 nm.

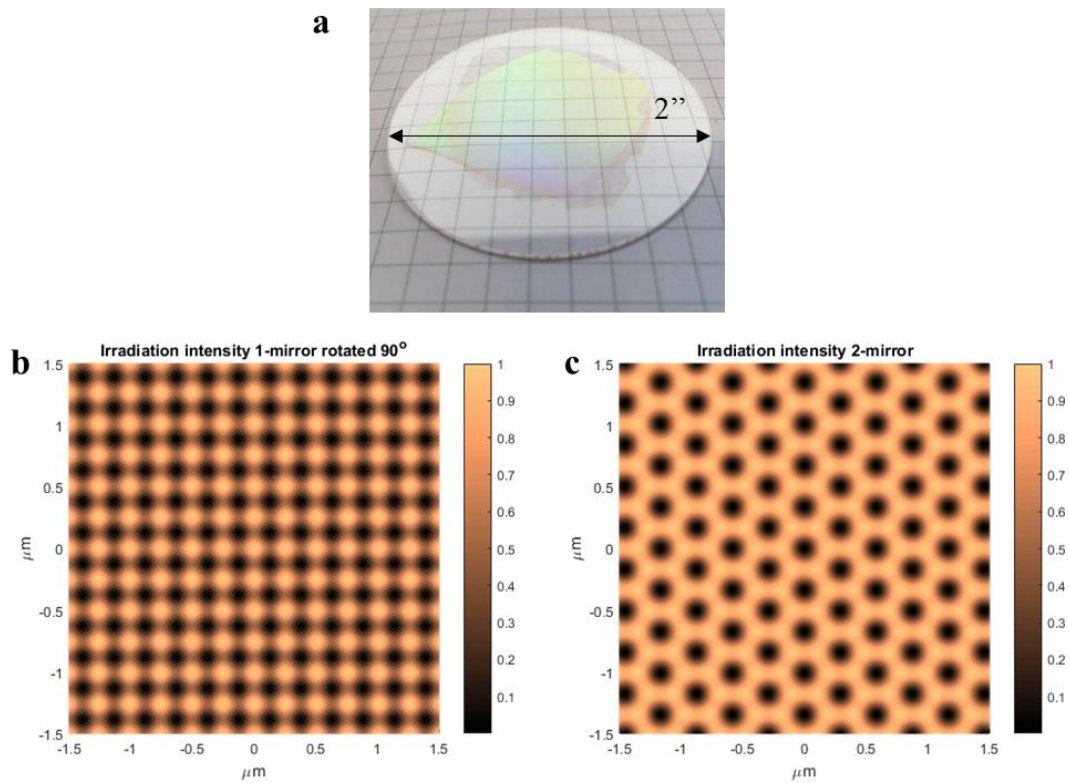


Figure S6. Laser interference lithography. (a) A photo of a LIL pattern generated on a two-inch fused silica wafer, demonstrating large area patterning. (b,c) Simulated intensity map for the Lloyd's interferometry with an incident angle of 40° set up for one-mirror (two-beam) system with a 90° sample rotation midway through exposure (b), and two-mirror (three beam) system (c).

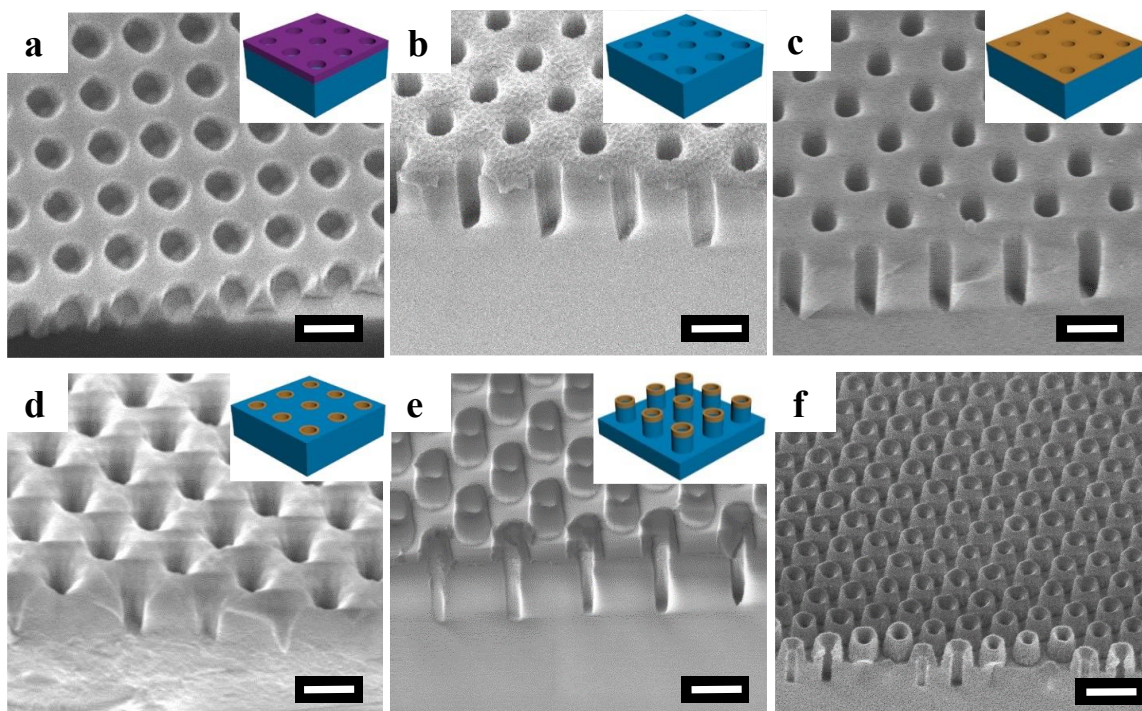


Figure S7. Corresponding SEM images (45° tilted) to the fabrication of nanotubes in glass. (a) Photoresist holes on SiO₂ substrate. **(b)** Etched nanohole arrays into SiO₂. **(c)** Nanoholes coated with 30 nm layer of Al₂O₃. **(d)** Breakthrough etch. **(e)** Further etch using the vertical deposition as a mask. **(f)** Additional glass nanotube example but with hexagonal arrangement. Scale bar = 500 nm.

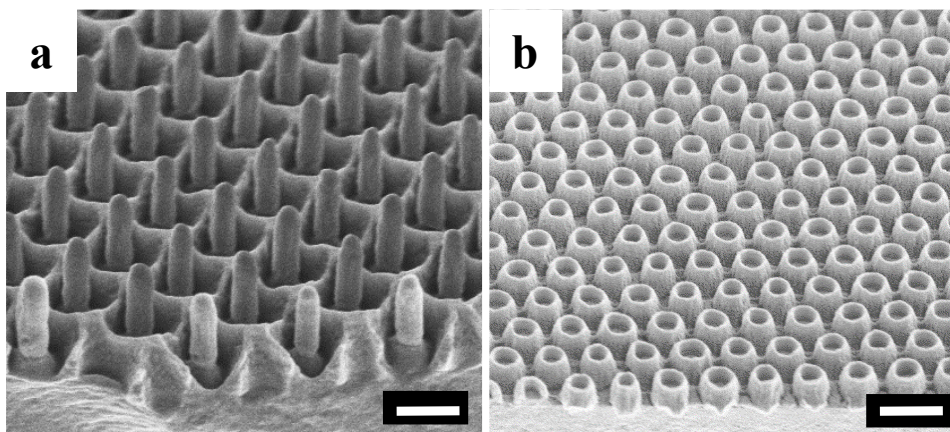


Figure S8. Representative nanotube structures imprinted in polymers. SEM images (45° tilted) of inverse nanotubes imprinted in polyurethane acrylate (PUA) *via* soft lithography (**a**), and photoresist nanotubes made *via* nanoimprint lithography (**b**). Scale bar = 500nm.

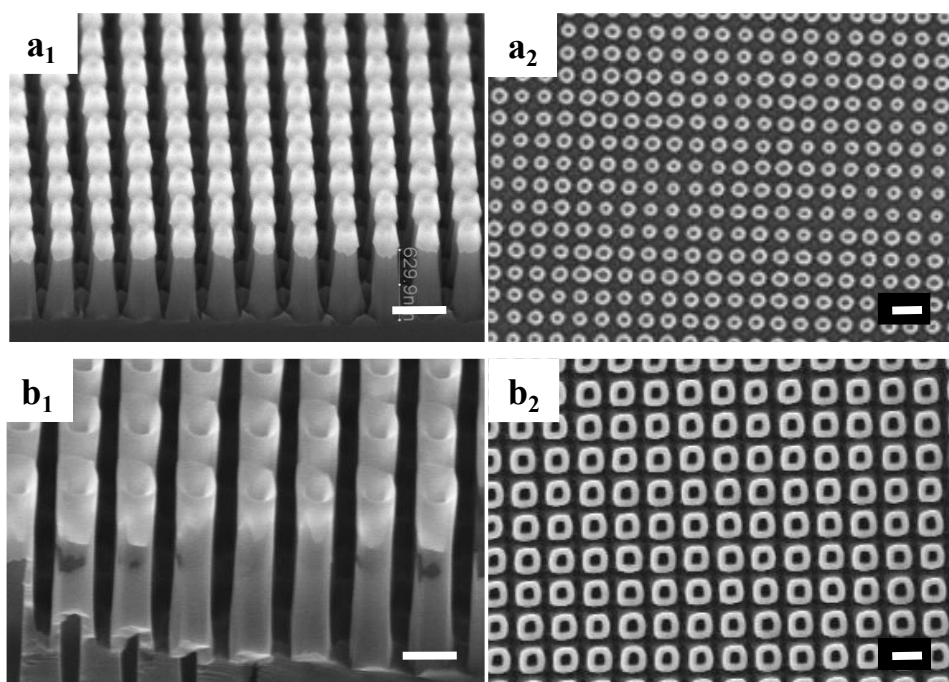


Figure S9. SEM images of nanotubes generated at two different pitches. (a) 350 nm pitch. (b) 560 nm pitch. Scale bars = 500 nm.

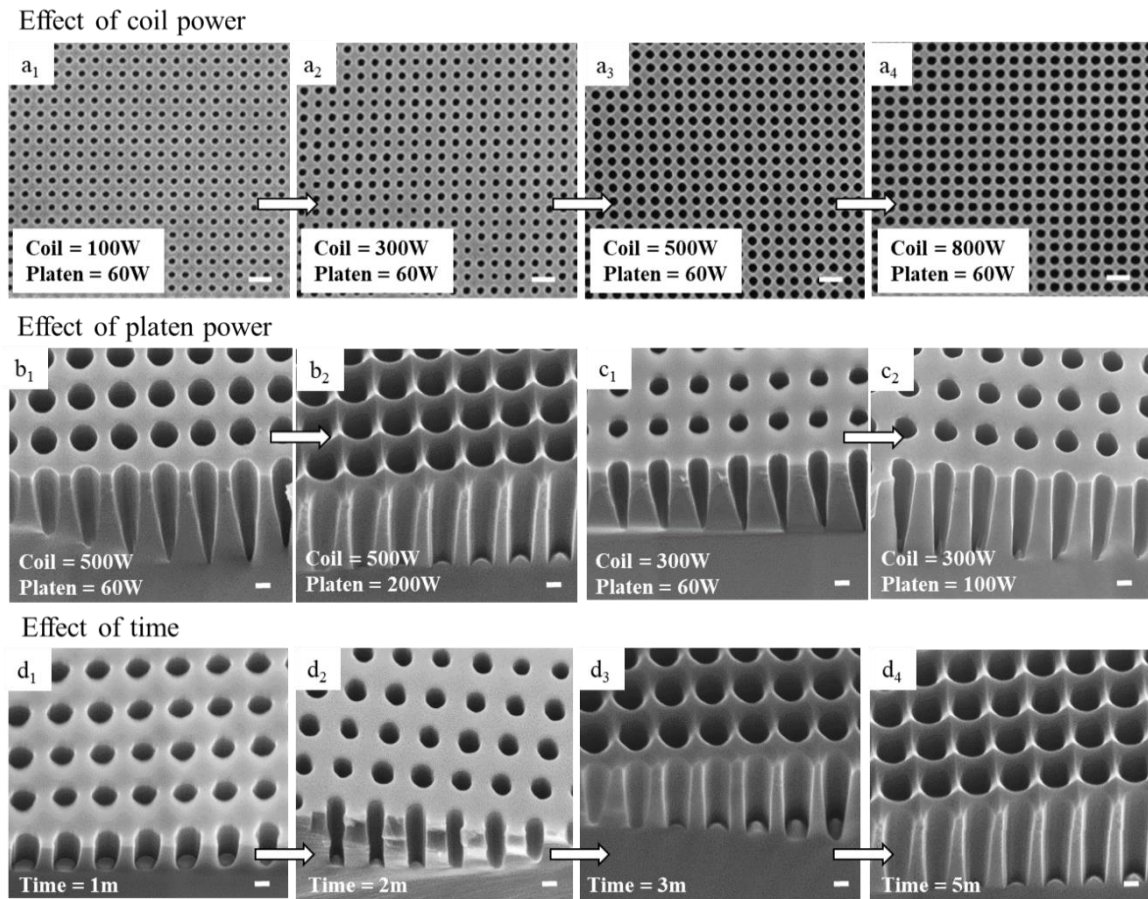


Figure S10. Investigation into the effect of coil power, platen power and time for the fabrication of the nanohole arrays in Si. (a) The effect of coil power is investigated starting from 100 W to 800 W at a constant platen power of 60 W for a time of 5 min. (b) The effect of platen power is investigated starting from 60 W to 200 W at constant coil power of 500 W and time 5 min. (c) The effect of platen power is investigated from 60 W to 100 W at constant coil power of 300 W and time 5 min. (d) The effect of time is investigated starting from 1 to 5 min at a constant coil power of 500 W and platen 200 W. Scale bar for (a) is 1 μm , for (b-d) is 200 nm.

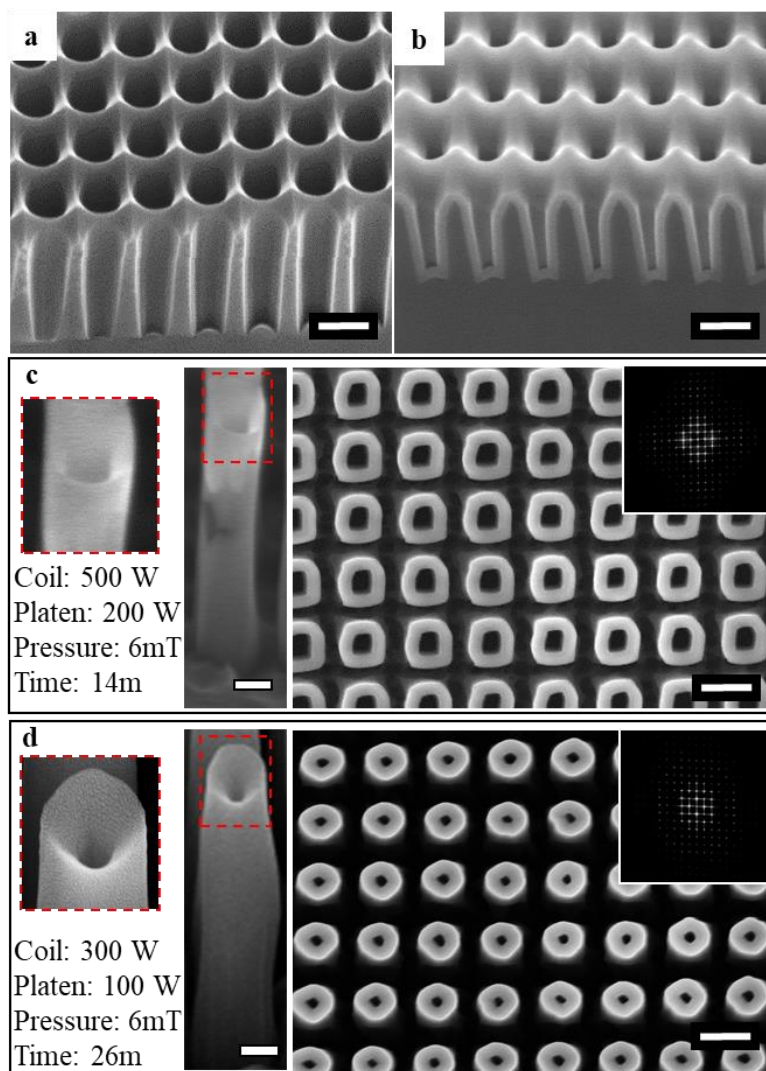


Figure S41. Tuning the transfer of the crown structure to the nanotube, and the outer and inner tapering. (a) SEM image of the nanohole array with crown structure present at the top. (b) SEM image of the same nanohole array with 90 nm layer of Al_2O_3 deposited. (c) Harsh and (d) mild etching conditions applied to (b) result in anisotropic or tapered etching of the inner and outer nanotube walls, respectively (side view SEM). Additionally, the post-ALD etching results in either removal (c) or preservation (d) of the crown (side and top view SEM.) The Fast Fourier Transform (FFT; inset), indicates that the order which originated from the LIL patterning, is preserved through to nanotube formation. Scale bars (a,b,d,f) = 500 nm, (c,e) = 200 nm.

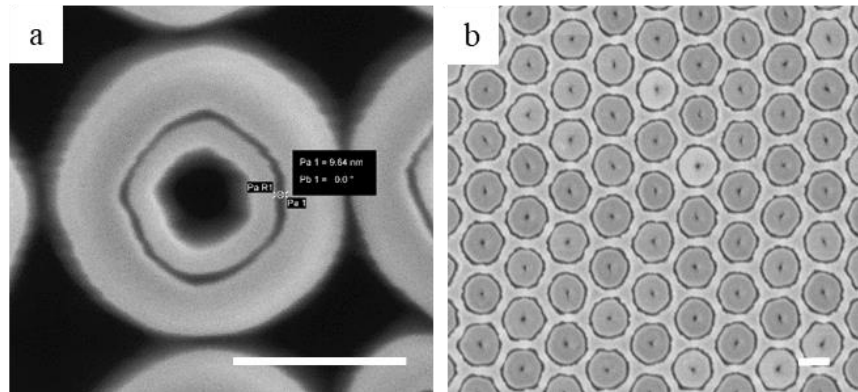


Figure S12. Further nanostructures generated through two SDIMP iterations. (a,b) Top view SEM images of nanostructures achieved with an incomplete final etch which led to very narrow gaps between the Al_2O_3 spacer layers; **(a)** Si concentric tubes with gap ~ 9 nm, **(b)** Glass embedded nano-doughnuts with gaps ~ 10 nm. Such narrow gaps are highly desired for application in optical trapping. Scale bar = 200 nm.

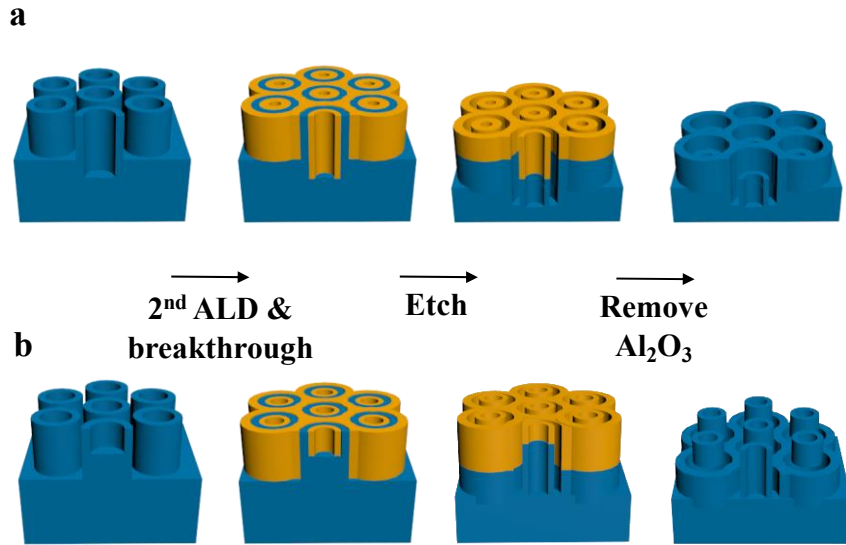


Figure S13. Schematics for the fabrication of hierarchical structures through two SDIMP iterations. (a) Starting from nanotubes that originated from nanoholes ($h_i > h_o$), the resultant structure after the second ALD and etch, comprises a shorter inner tube compared to the outer tube. (b) Starting from nanotubes that originated from nanopillars ($h_o > h_i$), the resultant structure after the second ALD and etch, comprises a taller inner tube compared to the outer tube.

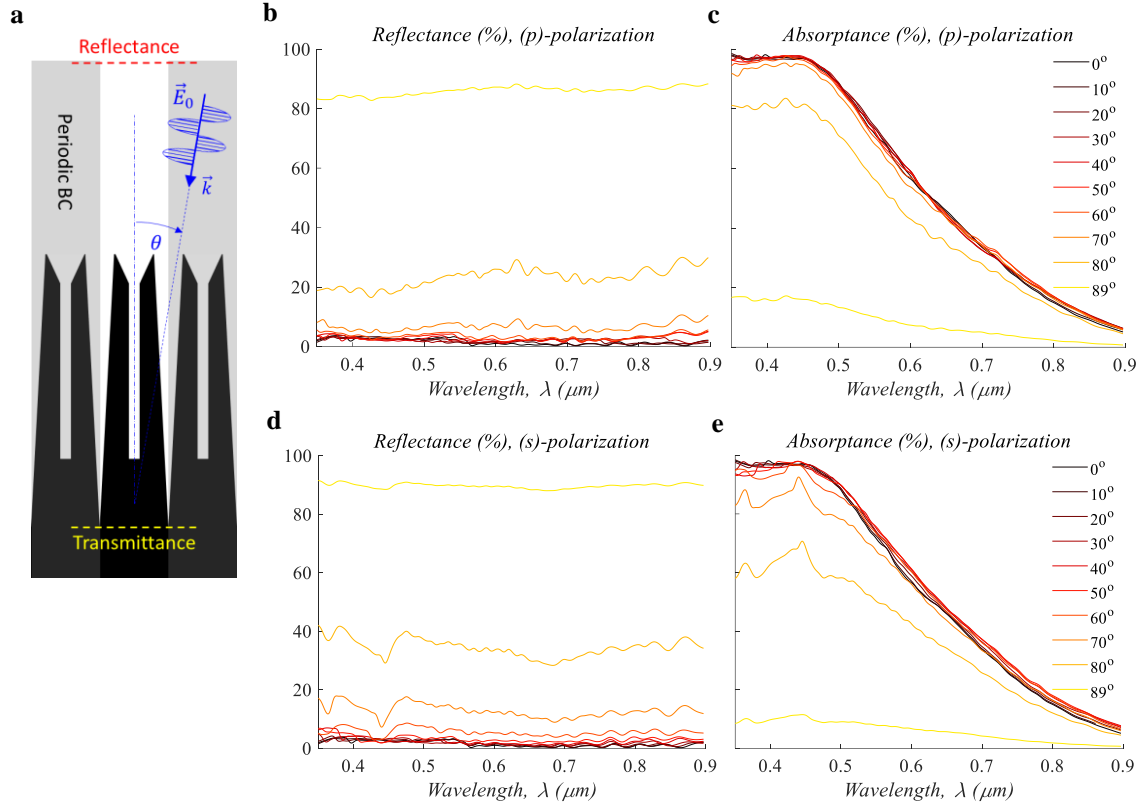


Figure S5. Optical properties of the tapered nanotube with a top crown at oblique angle of incidence. (a) Schematic of the simulation set up. The angle of incidence is defined by θ . Unless stated otherwise, light is polarized parallel to the plane of incidence (p-polarization). Periodic boundary conditions based on a square lattice were considered (gray shade). In order to quantify the absorption of Electromagnetic (EM) waves by the nanotubes, the power flux was monitored above and below the nanotubes, to measure reflection and transmission of EM-waves, respectively. (b) Reflectance and (c) Absorptance of p-polarized of EM waves as a function of the angle of incidence. (d) Reflectance and (e) Absorptance of s-polarized of EM waves as a function of the angle of incidence.

Supporting Tables

Table S1. Nanotube dimensions

Sample	Pitch (P) nm	Spacing (S) nm	Outer height, (h_o) nm	Inner height (h_i) nm	Thickness (t) nm	Inner tube radius (r_i) nm
Figure 1d	350	159 ± 9	800 ± 30	N/A	25	54 ± 6
Figure 2b	560	86 ± 12	893 ± 20	1623 ± 9	30	186 ± 16
Figure 2d	560	150 ± 15	1510 ± 20	1750 ± 14	90	89 ± 5
Figure 2e	350	0	370 ± 8	N/A	120	55 ± 7
Figure 2f	350	0	455 ± 11	N/A	120	109 ± 8
Figure 2h	560	162 ± 14	1721 ± 16	1743 ± 11	30	143 ± 11
Figure 2j	560	168 ± 18	1224 ± 14	2302 ± 17	30	147 ± 6

Table S2. Nanotube fabrication: (i) etching times and (ii) thicknesses of SiO₂ or Al₂O₃ deposition

Sample	SiO ₂ thickness / nm	O ₂ etch / s	CHF ₃ /Ar etch / min	Cl ₂ etch / min	t ALD / nm	Cl ₂ etch / min
Figure 1d	70	8	3.5	4	25	8
Figure 2b	200	10	9	5	30	9
Figure 2d	200	10	9	15	90	14
Figure 2e	70	30	1.5	3	150	17
Figure 2f	70	30	1.5	3	120	16
Figure 2h	200	10	9	15	30	5
Figure 2j	200	10	9	5	30	16

Table S3. Nanotube etching conditions – Oxford RIE

Oxford RIE conditions – capacitively coupled plasma					
Oxygen breakthrough	Pressure / mTorr		RF Power / W		O₂ / sccm
	50		100		50
SiO₂ etch	Pressure /mTorr		RF Power / W	CHF₃ / sccm	Ar /sccm
	50		200	12	38

Table S4. Nanotube etching conditions – ICP STS

Sample	1 st Si etch				Breakthrough etch				Further etch			
	Coil /W	Platen /W	P /mTorr	t /min	Coil /W	Platen /W	P /mTorr	t /min	Coil /W	Platen /W	P /mTorr	t /min
Figure 1d	300	40	6	4					300	40	6	8
Figure 1e	500	200	6	5	300	40	3	9	500	200	6	5
Figure 2b	500	200	6	5	300	40	3	3	300	100	6	6
Figure 2d	500	200	6	5	300	40	3	9	500	200	6	5
Figure 2e	300	40	6	3					300	40	6	17
Figure 2f	300	40	6	3					300	40	6	16
Figure 2h	500	60	6	15	300	40	3	3	500	200	6	5
Figure 2j	300	100	6	5					300	100	6	16

Table S5. Tunability at each step of the SDIMP process

Step in the fabrication process	Parameters that can be tuned		
	Pitch (P) and spacing (S)	Shape	Height
<p>Step 1 Etch mask fabrication (LIL)</p> <ul style="list-style-type: none"> • Exposure time • Rotation angle • Development time 	<p>Changing the mirror angle changes the pitch according to the following equation (for a one mirror system), where λ is the wavelength of the laser and θ is the mirror angle</p> $P = \frac{\lambda}{2 \sin \theta}$	<p><u>With a one-mirror system:</u> the angle of sample rotation (typically 60° or 90°) gives hcp ellipsoidal or square packed circular pillars or holes.</p> <p><u>With a two-mirror system:</u> hcp circular holes/pillars. Exposure and development time can make the holes/pillars smaller or larger.</p>	<p>Thickness of the photoresist impacts the height of the etched structures.</p> <p>Morphology of the etch mask (holes/pillars) influences the inner and outer nanotube height.</p>
<p>Step 1 Oxygen breakthrough</p>	<p>Cannot affect pitch, but can increase or decrease the spacing for nano-pillars/holes, respectively.</p>	<p>Increasing the oxygen breakthrough time results in pillars with a reduced diameter or holes with an increased diameter.</p>	<p>Increasing the oxygen breakthrough time reduces the height of the photoresist mask.</p>
<p>Step 2 SiO₂ hard mask etching</p>		<p>The shape of the hard mask can be altered through the gas ratios, platen power and pressure.</p>	<p>The thickness of the deposited SiO₂ layer dictates the height of the hard mask. Higher aspect ratio structures in Si are possible with taller hard mask.</p>
<p>Step 3 Si etching</p>		<p>Altering the coil/platen power in ICP RIE system and etching time all have a distinct effect on the end shape of the nanotubes. The differences are most notable during Step 3 (Si etch from SiO₂ hard mask to obtain nanoholes or nanopillars in Si).</p>	<p>Harsher etching conditions result in higher etch rates (increased coil/platen power).</p> <p>Longer etching times result in taller structures.</p>

		Figure S10 shows SEM images of the structures obtained by independently altering the coil/platen power and time.	
Step 4 SDIMP ALD		<p><u>Single nanotube:</u> For pillars, increasing the ALD thickness increases the outer diameter of the tube, whereas for holes it decreases the inner diameter of the tube</p> <p><u>Concentric:</u> Combinations of different ALD thicknesses for the 1st and 2nd deposition provide access to a vast number of possible end structures.</p>	The height of the vertical ALD is determined by the height of the sacrificial pattern. Evidently deeper/taller nano-holes/pillars result in taller nanotubes after SDIMP. This also has an impact on the inner/outer tube height and can be tuned accordingly.
Steps 5-6		The post-ALD etching conditions have a significant impact on the nanotube morphology as can be seen in Figure S11.	Post-ALD etching is a key stage at which to tune the height. Etching until mask consumption is possible, otherwise the remaining mask is removed by HF.

Table S6. Etching rates of single nanotubes starting from nanopillars corresponding to Figure 1. The etching rates were determined by linear fit.

Nanopillar starting point		
	Silicon	Al₂O₃
Etch rate / nm/min	154 ± 17	8 ± 2

The process times for the structures fabricated through the double iteration of SDIMP are listed in Table S7. The conditions for the SiO₂ etch were maintained the same (Table S3) and ICP etching conditions were maintained at Coil = 300 W, Platen = 40 W, Pressure = 6 mTorr for all samples.

Table S7. Iterative SDDP structure fabrication

Sample	SiO₂ thickness /nm	O₂ / s	CHF₃/Ar etch / min	Cl₂ etch / min	ALD / nm	Cl₂ etch / min	ALD / nm	Cl₂ etch / min
Figure 3b	70	38	1.5	3	40	7	25	11.5
Figure 3c	70	40	1.5	2	60	9	80	14
Figure 3e	70	45	1.7	1	45	7.5	30	6
Figure 3g	70	30	1.5	3	120	16	30	5
	O₂ / s	CHF₃/Ar etch / min	ALD / nm	Cl₂ etch / min	CHF₃/Ar etch / min	ALD / nm	Cl₂ etch / min	CHF₃/Ar etch / min
Figure 3i	12	10	40	3	10	30	3	10

Note, the longer oxygen breakthrough times result from starting with a PR pattern (holes/pillars) generated from NIL as opposed to LIL.

References

- (1) Dallorto, S.; Staaks, D.; Schwartzberg, A.; Yang, X.; Lee, K. Y.; Rangelow, I. W.; Cabrini, S.; Olynick, D. L. Atomic Layer Deposition for Spacer Defined Double Patterning of Sub-10 Nm Titanium Dioxide Features. *Nanotechnology* **2018**, *29*, 405302.
- (2) Korre, H.; Fucetola, C. P.; Johnson, J. A.; Berggren, K. K. Development of a Simple, Compact, Low-Cost Interference Lithography System. *J. Vac. Sci. Technol. B, Nanotechnol. Microelectron. Mater. Process. Meas. Phenom.* **2010**, *28*, C6Q20-C6Q24.
- (3) Williams, K. R.; Gupta, K.; Wasilik, M. Etch Rates for Micromachining Processing - Part II. *J. Microelectromechanical Syst.* **2003**, *12*, 761–778.
- (4) Jung, H.; Shin, W. H.; Park, T. W.; Choi, Y. J.; Yoon, Y. J.; Park, S. H.; Lim, J.-H.; Kwon, J.-D.; Lee, J. W.; Kwon, S.-H.; Seong, G. H.; Kim, K. H.; Park, W. I. Hierarchical Multi-Level Block Copolymer Patterns by Multiple Self-Assembly. *Nanoscale* **2019**, *11*, 8433–8441.
- (5) Norasethekul, S.; Park, P. Y.; Baik, K. H.; Lee, K. P.; Shin, J. H.; Jeong, B. S.; Shishodia, V.; Lambers, E. S.; Norton, D. P.; Pearton, S. J. Dry Etch Chemistries for TiO₂ Thin Films. *Appl. Surf. Sci.* **2001**, *185*, 27–33.
- (6) Shkondin, E.; Takayama, O.; Lindhard, J. M.; Larsen, P. V.; Mar, M. D.; Jensen, F.; Lavrinenko, A. V. Fabrication of High Aspect Ratio TiO₂ and Al₂O₃ Nanogratings by Atomic Layer Deposition. *J. Vac. Sci. Technol. A Vacuum, Surfaces, Film.* **2016**, *34*, 031605.
- (7) Ashkin, A.; Dziedzic, J. M.; Bjorkholm, J. E.; Chu, S. Observation of a Single-Beam Gradient Force Optical Trap for Dielectric Particles. *Opt. Angular Momentum* **1986**, *11*, 288.
- (8) Neuman, K. C.; Block, S. M. Optical Trapping. *Rev. Sci. Instrum.* **2004**, *75*, 2787–2809.
- (9) Saleh, A. A. E.; Dionne, J. A. Toward Efficient Optical Trapping of Sub-10-Nm Particles with Coaxial Plasmonic Apertures. *Nano Lett.* **2012**, *12*, 5581–5586.
- (10) Yoo, D.; Gurunatha, K. L.; Choi, H. K.; Mohr, D. A.; Ertsgaard, C. T.; Gordon, R.; Oh,

- S. H. Low-Power Optical Trapping of Nanoparticles and Proteins with Resonant Coaxial Nanoaperture Using 10 Nm Gap. *Nano Lett.* **2018**, *18*, 3637–3642.
- (11) Miyazaki, H. T.; Kurokawa, Y. Squeezing Visible Light Waves into a 3-Nm-Thick and 55-Nm-Long Plasmon Cavity. *Phys. Rev. Lett.* **2006**, *96*, 097401.
- (12) Nagpal, P.; Lindquist, N. C.; Oh, S.-H.; Norris, D. J. Ultrasooth Patterned Metals for Plasmonics and Metamaterials. *Science.* **2009**, *325*, 594–597.